Applied Catalysis B: Environmental 234 (2018) 198–205

Contents lists available at ScienceDirect

Applied Catalysis B: Environmental

journal homepage: www.elsevier.com/locate/apcatb

Hydrogen bonds in heterojunction photocatalysts for efficient charge transfer

Zhengyuan Jin[a,b,c], Qitao Zhang[c], Jiaqi Chen[a], Shaolong Huang[a], Liang Hu[a], Yu-Jia Zeng[a,*], Han Zhang[c,*], Shuangchen Ruan[a], Teruhisa Ohno[b,*]

[a] Shenzhen Key Laboratory of Laser Engineering, College of Optoelectronic Engineering, Shenzhen University, Shenzhen, 518060, PR China
[b] Department of Applied Chemistry, Faculty of Engineering, Kyushu Institute of Technology, 1-1 Sensuicho, Tobata, Kitakyushu 804-8550, Japan
[c] International Collaborative Laboratory of 2D Materials for Optoelectronics Science and Technology, College of Optoelectronic Engineering, Shenzhen University, Shenzhen, 518060, PR China

ARTICLE INFO

Keywords:
Graphitic carbon nitride
Melamine cyanurate
Hydrogen bond
Charge transfer
Photocatalysis

ABSTRACT

A hydrogen bond-based heterojunction photocatalyst, g-C_3N_4/melamine-cyanurate (gMC), was synthesized by a facile alkaline hydrothermal approach. The hydrogen bonds between the two substrates (N—HO═C) provide not only an ultrafast pathway (hundreds of femtoseconds) but also an inner electric field for hole transfer from g-C_3N_4 to melamine-cyanurate. Although only the g-C_3N_4 moiety acts as a photocatalyst, the optimized composite presents approximately 5.4, 3 and 2.5 times higher photocatalytic activity than bulk g-C_3N_4 in the decomposition of acetaldehyde and 2-propanol and the generation of H_2 by water splitting, respectively. In this paper, we demonstrate that hydrogen bonds can not only lower the interfacial barrier and separate redox sides but also control the direction of charge transfer, which enables the design of the photocatalytic mechanism.

1. Introduction

The development of heterojunction composite photocatalysts is one of the most effective ways to harvest energy from the visible-light region and to improve the photocatalytic activity [1–3]. The interfacial barrier between two substances in a heterojunction photocatalyst is the bottleneck for charge transfer, both in the Z-scheme and charge separation mechanisms, which are most used in heterojunction photocatalysis. The van der Waals force is not strong enough at such distance to lower the interfacial barrier to efficiently transfer charge. Several strategies have been reported to lower the interfacial barrier, such as loading noble metals or graphene between two substances [4,5], the formation of p-n heterojunctions [6], and the introduction of ions in solution as a redox agent [7].

Here, we present a novel method to lower the interfacial barriers, namely, through hydrogen bonding. Hydrogen bonding is a type of force with a strength between the van der Waals force and a chemical bond that widely exists in nature [8]. Research into hydrogen bonding can be easily found in many branches of science [9]. Although electron transfer though a hydrogen bond in a single DNA base pair and a better conduction in a hydrogen bond as compared to that in a covalent σ bond have been reported [10,11], very limited reports about the hydrogen bonding can be found in photocatalysis until recently [12,13]. These reports have examined the hydrogen bonds between the photocatalyst and organic compounds (such as benzylalcohol) to explain the mechanism of the improved photocatalytic activity of photodecomposition. Since many new types of strong and unconventional hydrogen bonds have been identified in the liquid phase as well as the solid state [8,14], the aim of this study is to suggest a hydrogen bond is perhaps an excellent constitution for development of composite photocatalysts.

Melamine-cyanurate (MC) contains oxygen in its frame and is constituted by melamine and cyanuric acid. MC is commonly used as a precursor for synthesizing g-C_3N_4 samples with unique architecture, such as hollow spheres, sheets and tubes [15,16].

In this paper, we report a facile hydrothermal method and the successful synthesis of g-C_3N_4/melamine-cyanurate (gMC), which has high photocatalytic activity towards the photodecomposition of gaseous organics as well as water splitting for H_2 generation under visible-light irradiation. gMC reveals a higher photocatalytic activity than bulk g-C_3N_4 under visible-light irradiation, although it has a low specific surface area and a blueshifted light absorption. In the gMC complex, the hydrogen bonds between g-C_3N_4 and melamine-cyanurate play a key role in the improvement of the photocatalytic activity. The two ends of the N—HO═C hydrogen bonds provide the driving force for the transfer of photoexcited electrons from MC to g-C_3N_4. This behavior is

* Corresponding authors.
E-mail addresses: yjzeng@szu.edu.cn (Y.-J. Zeng), hzhang@szu.edu.cn (H. Zhang), tohno@che.kyutech.ac.jp (T. Ohno).

https://doi.org/10.1016/j.apcatb.2018.04.057
Received 15 January 2018; Received in revised form 16 April 2018; Accepted 22 April 2018
Available online 22 April 2018
0926-3373/

analogous to Z-scheme, in which photoexcited holes transfer from the valence band to a deeper band. Moreover, since the oxidation site changes from the nitrogen of g-C_3N_4 to the oxygen of melamine-cyanurate, the redox sites are separated, which reduces the recombination of photoexcited electrons and holes.

2. Experimental procedures

2.1. Materials

Melamine (Wako Pure Chemical Industries, Ltd.), ammonia solution (25%) (Wako Pure Chemical Industries, Ltd.), dimethyl sulfoxide (DMSO) (Wako Pure Chemical Industries, Ltd.) and cyanuric acid (98%) (Sigma-Aldrich) were used as received without further treatment.

2.2. Characterization

Characterization was performed by using an X-ray diffractometer (Rigaku, MiniFlex II) with CuKα radiation (λ = 1.5405 Å). Morphology of the prepared samples were observed by a field emission scanning electron microscope (FE-SEM; JEOL, JSM-6701FONO) and a transmission electron microscopy (TEM; Hitachi H-9000NAR). Diffuse reflectance spectra (DRS) were measured using a UV–vis spectrophotometer (Shimadzu, UV-2600) equipped with an integrating sphere unit (Shimadzu, ISR-2600 Plus). Specific surface area (S_{BET}) and poresize/volume were determined with a surface area analyzer (Quantachrome, Nova 4200e) by the Brunauer-Emmett-Teller (BET) and Barrett-Joyner-Halenda (BJH) method. Functional group vibrations were confirmed by using a Fourier transform infrared spectrometer (FTIR; JASCO, FT/IR 4200) with a diffuse reflectance accessory (JASCO, DR-81), and the in-situ FTIR was performed by FTIR (VERTEX 70v) with a high temperature and pressure cell (Specac). Fluorescence spectrophotometer (Edinburgh Instruments FLS-920; 365 nm as incident light source) was used to determine photoluminescence and the time-resolved fluorescence decay. Surface chemical states were investigated by X-ray photoelectron spectroscopy (XPS) measurement with Thermo Scientific ESCALAB 250Xi system by Al Karadiation and adventitious C1s peak (284.6 eV) as the reference. Fluorescence spectrophotometer (Edinburgh Instruments FLS-920; 405 nm as incident light source) was used to determine photoluminescence and the time-resolved fluorescence decay. Thermogravimetric (TG) analysis was measured by using Rigaku TG-TDA-8120H. Solid-state NMR studies were performed with a Bruker AvanceII spectrometer operating at 400 MHz ^{1}H Lamor frequency. The ^{1}H spectra were recorded using a standard Bruker 4 mm double-resonance MAS probe. The samples were rotated with a spinning frequency of 14 kHz. For ^{1}H single pulse MAS experiments, the 900 pulse length was 2.5 us, and the recycle delay was 25 s.

2.3. Synthesis of g-C_3N_4, g-C_3N_4/melamine-cyanurate and melamine-cyanurate

G-C_3N_4 powders were synthesized by heating 30 g of melamine at 823 K with a heating rate of 9 K min^{-1} and kept for 4 h. The products were collected and grounded into powders. The sample is denoted as bulk g-C_3N_4.

G-C_3N_4/melamine-cyanurate was synthesized by hydrothermal treatment of g-C_3N_4 in alkaline solution as follows. Ammonia solution (Wako 25%, 2 ml, 5 ml and 10 ml) was added in 50 ml deionized-water, respectively. One gram of g-C_3N_4 was dispersed in above solution by ultrasonication for 10 min and stirring of 1 h. Then it was heated in Teflon-lined autoclave at 200 °C for 6 h. Light yellow powder was obtained after filtration and evaporation. The samples were denoted as gMC2, gMC5 and gMC10 corresponding to the added volume of ammonia solution 2 ml, 5 ml and 10 ml, respectively.

Melamine-cyanurate was fabricated as follows. Five hundred milligram of melamine and 500 mg of cyanuric acid were dissolved in 20 ml and 10 ml of dimethyl sulfoxide, respectively, with sonication. Both solutions were mixed together for 10 min to give white precipitates. Subsequently, the sample was filtered and washed with ethanol several times, followed by evaporation.

2.4. Performance analysis

2.4.1. Photodecomposition of acetaldehyde and 2-propanol

Before evaluation of the photocatalytic activity, each sample was irradiated with UV light using black light (UVP, XX-15BLB) in order to remove organic contaminants on the sample. The photocatalytic activity of the sample was evaluated by CO_2 liberation from photodecomposition of acetaldehyde. One hundred milligrams of powder, which has complete extinction of incident radiation, was spread on the bottom of glass dish, and the glass dish was placed in a Tedlar bag (AS ONE Co. Ltd.). Then 125 cm^3 artificial air containing 500 ppm of acetaldehyde was injected into the bag. Photoirradiation was performed at room temperature after the acetaldehyde had reached adsorption equilibrium. A light-emitting diode (LED; Epitex, L435-30M32L, ca. 435 nm, 3.0 mW cm^{-2}) was used as a light source. The concentrations of acetaldehyde and CO_2 were collected by on-line gas chromatography (Agilent Technologies, 3000A Micro-GC, TCD detector) equipped with OV1 and PLOT-Q columns as a function of irradiation time. Photodecomposition of 2-propanol was evaluated by the same procedure as acetaldehyde.

2.4.2. Photocatalytic hydrogen generation from water splitting

The photocatalytic activities were evaluated by photocatalytic generation of H_2 from water splitting with λ ≥ 420 nm light (Xenon lamp, CEAULIGHT, CEL-HXF300; optical filter CEAULIGHT, CEL-UVIRCUT420). Reactions were carried out in a Pyrex top-irradiation reaction vessel connected to a closed glass gas system (CEAULIGHT, CEL-SPH2N). Typically, 10 mg of samples were dispersed in 100 ml deionized water, which contains 10 vol % of triethanolamine (TEOA) and 3 wt% (respect to Pt) $H_2PtCl_6.6H_2O$. The solution was irradiated by the light with the intensity of 100 mW cm^{-2} after the air was completely removed in the system. The temperature of the solution was maintained at 12 °C. The evolved gases were analyzed by gas chromatography (CEAULIGHT, GC-7920) using N_2 as the carrier gas.

2.4.3. Photoelectrochemical measurements

The sample was fabricated on FTO substrates by an electrophoresis method. 10 mg of the sample and a spot of iodine were ultrasonically dispersed in 20 ml acetone solution. Two FTO conducting glasses were placed in the solution as the anode and the cathode. A bias of 15 V was applied between two electrodes using a direct current power supply for 3 min (3 times). Sample loaded FTO was then dried. Linear sweep voltammetry and chronoamperometry measurements were carried out by using an automatic polarization system (HSV-100, Hokuto Denko Co.) with a three-electrode system, in which the prepared electrode, a Pt and a Ag/AgCl electrode were used as the working electrode, counter electrode and reference electrode, respectively. 0.5 M Na_2SO_4 solution was used as the electrolyte. The light source was an AM 1.5 G solar-simulated system (PEC-L15, Peccell Tech., Inc.). The light intensity of the solar-simulated light was adjusted to 100 mW cm^{-2} by utilizing a thermopile power meter (ORION-TH). The linear sweep voltammogram (LSV) was scanned in the anodic direction at a scan rate of 10 mV s^{-1}.

3. Results and discussion

Direct evidence for the formation of MC can be confirmed in the XRD patterns and FTIR spectra shown in Fig. 1a and b. It can be determined that with a higher concentration of ammonia solution, both the XRD patterns and FTIR spectra become more similar to that of MC. Fig. 1a shows the XRD patterns of the samples. After hydrothermal

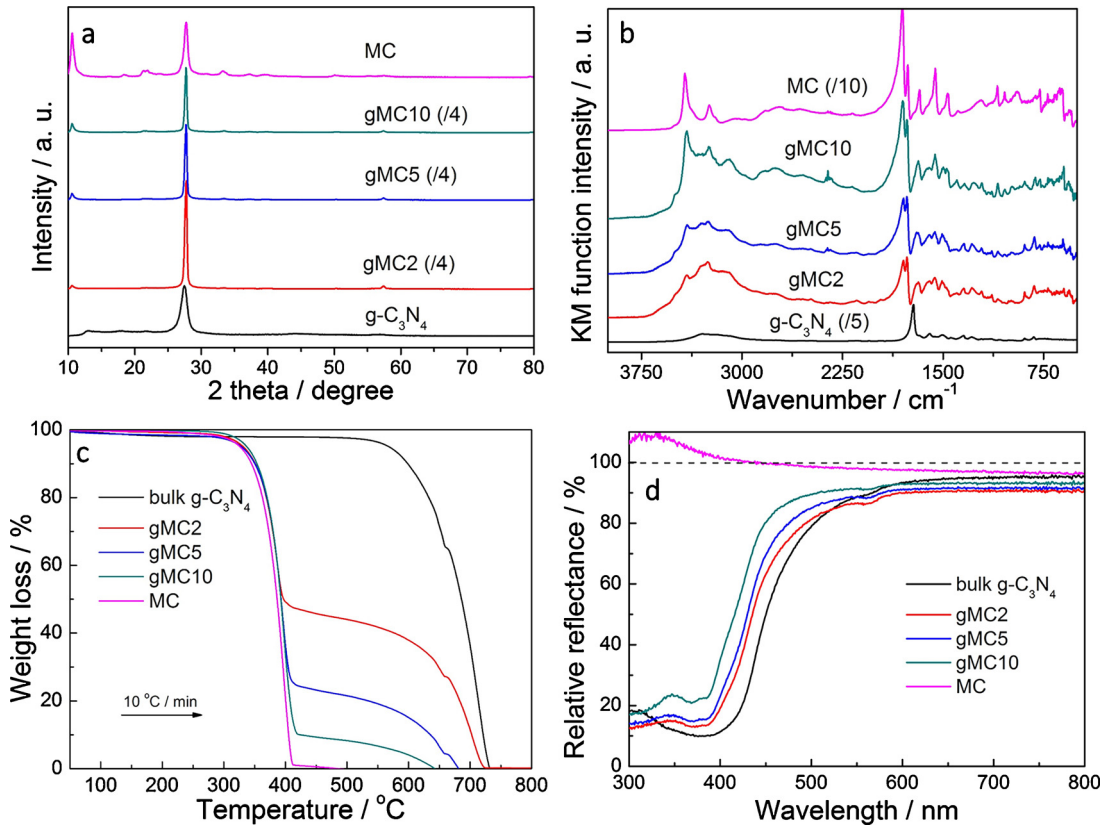

Fig. 1. (a) XRD patterns and (b) FTIR spectra of bulk g-C_3N_4 and gMC samples. The intensity of gMC2, gMC5 and gMC10 reduced to 1/4 in the XRD patterns; the intensity of g-C_3N_4 and MC reduced to 1/5 and 1/10 in the FTIR spectra, respectively.

treatment, the peak at 13.1° in the pattern of bulk g-C_3N_4 disappeared, and new peaks at 10.6, 18.3, 21.3 and 33.4° appeared, which are the characteristic peaks of MC [14]. Moreover, the strong peak at 27.4° in bulk g-C_3N_4 shifts to 27.7°, which exactly corresponds to the MC pattern. Analogous results can be found in the FTIR spectra in Fig. 1b. Peaks in the region from 900 to 1800 cm^{-1}, attributed to either trigonal C—N(—C)—C or bridging C—NH—C units, are observed in all samples. In the region between 1750–2100 cm^{-1} in the spectra of the gMC samples, two peaks originating from C═O vibrations appear, which can also be found in the MC spectrum [16]. Moreover, the peak at approximately 1600 cm^{-1} sharply decreased as the ammonia concentration increased in the gMC samples. From these results and the TG analysis results (Fig. 1c), we can confirm that unstable MC formed, which is easier to decompose (ca. 275 °C) than g-C_3N_4. On the other hand, g-C_3N_4 still exists, even in gMC10 [15,16]. Moreover, introducing a higher concentration of ammonia solution can promote the generation of MC. From the above results, it can be concluded that after hydrothermal treatment, a g-C_3N_4/MC composite was obtained. Fig. 1d shows the UV–vis diffuse reflectance spectra (DRS) of the samples. Compared to the spectrum of bulk g-C_3N_4, the spectra of the obtained samples were blueshifted with an increase in the concentration of ammonia solution. This can be expected as MC presents as a white powder that cannot absorb any light between 300 nm and 800 nm.

A scanning electron microscope (SEM) was employed to investigate the textural structure and morphology of the samples, as shown in Fig. 2. Bulk g-C_3N_4 displays a typical stacked lamellar structure. Compared with the sheet-like morphology of bulk g-C_3N_4, the obtained samples showed a rod-like morphology, and the diameters of the nanorods increased to approximately 500 nm, 700 nm and 2 μm as the concentration of the ammonia solution increased. That is the reason why the specific surface area decreased (Table 1). A transmission electron microscope (TEM) was used to further investigate the textural structure and morphology, as shown in Fig. 2e and f. Compared with the smooth surface of bulk g-C_3N_4, the surface of gMC was obviously bumpy. It can be seen from the nitrogen adsorption isotherms and pore size distributions calculated from the desorption branch by the Barrett-Joyner-Halenda (BJH) method (Figs. S1 and S2) that with increasing ammonia content, the mesoporous (ca. 2 nm) part of the obtained gMC decreased dramatically, which is also the cause of the decrease in the specific surface area.

Elemental analysis revealed a C/N molar ratio of 0.66 and less than 2 wt% H in bulk g-C_3N_4. As the concentration of the ammonia solution increased, the C and N content decreased, while the O and H content increased (Table 1). Moreover, the pH of the solution became higher after hydrothermal treatment, indicating that MC resulted from the breakage of g-C_3N_4 during the hydrothermal reaction. To determine the distribution of MC in the gMC sample, gMC was again calcined at 550 °C for 4 h. In contrast to the results shown in Fig. S4a, we obtained mesoporous g-C_3N_4 after the second calcination (Fig. S3b). The results suggest that MC may exist in the g-C_3N_4 framework and the two compounds are not obviously separated. This is the reason why gMC10 exhibits an almost two times higher activity than the ground sample, which will be discussed later.

The photocatalytic activities of the prepared samples were evaluated by the amount of CO_2 and acetone liberated from the photodecomposition of acetaldehyde and 2-propanol, respectively. Fig. 3a shows the time evolution of CO_2 generated by the obtained samples. As the concentration of the ammonia solution increased, the photocatalytic activity increased gradually. In other words, the photocatalytic activity of gMC increases with increasing MC content in the gMC system. gMC2 and gMC5 generated 162.3 ppm and 256.5 ppm of CO_2, respectively. gMC10 exhibited the highest photocatalytic activity, which is almost 5.4 times (445.6 ppm) higher than that of bulk g-C_3N_4 (82.9 ppm). The descending tendencies of acetaldehyde variation

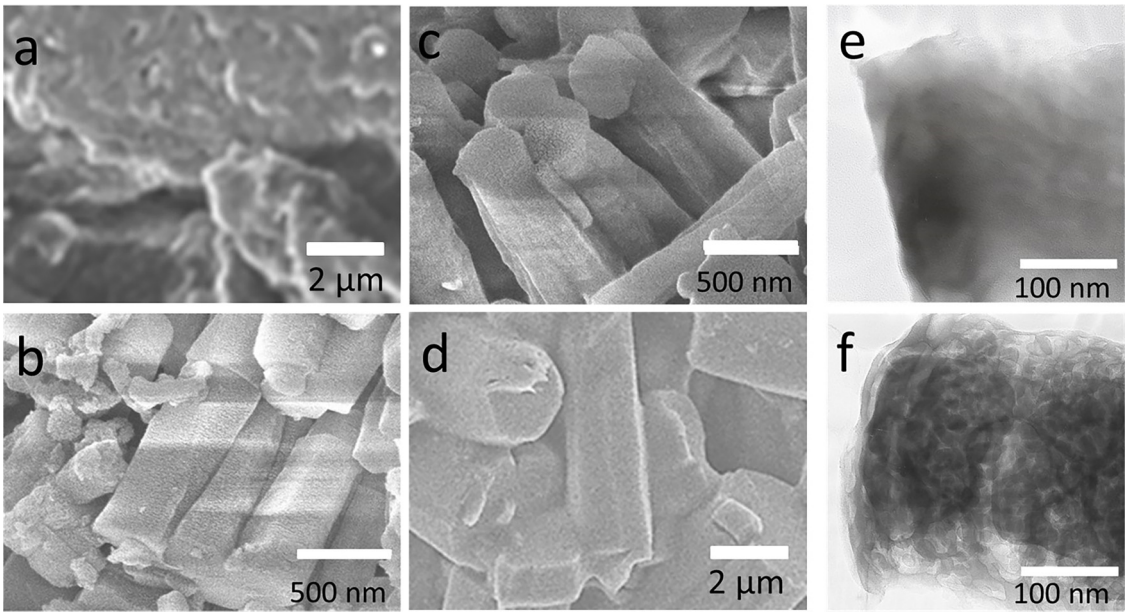

Fig. 2. SEM images of (a) bulk g-C_3N_4, (b) gMC2, (c) gMC5 and gMC10. TEM images of (c) bulk g-C_3N_4 and (f) gMC10.

Table 1
Specific surface area and elemental analysis of the samples obtained after hydrothermal treatment in different concentrations of ammonia solution.

	$S_{BET}(m^2/g)$	C(wt%)	N(wt%)	H(wt%)	O(wt%)	C/Nmolar ratio
bulk g-C_3N_4	11.4	34.7	61.4	1.9	1.9	0.659
gMC2	20.3	30.3	54.1	2.8	12.7	0.654
gMC5	11.7	29.2	52.0	3.1	15.6	0.655
gMC10	6	28.5	50.5	3.3	17.6	0.659

curves (Fig. S4) agreed with the photocatalytic activity of CO_2 generation. Figs. 3b, S5a and b show the time evolution of acetone generated, the descending tendencies of 2-propanol variation curves and time evolution of CO_2 generated, respectively. After 18 h irradiation, gMC10 released 346.0 ppm of acetone, which is 3 times higher than that of bulk g-C_3N_4 (110.4 ppm). Simultaneously, in Fig. S5, gMC10 shows the higher decomposition rate of 2-propanol and released almost 2 times higher CO_2 (94.4 ppm) than that of bulk g-C_3N_4 (50.1 ppm). In blank experiment, gMC10 generated 18.7 ppm of CO_2 after 23.5 h irradiation, which not only suggests CO_2 mostly generated from decomposition of acetaldehyde, 2-propanol and acetone in above experiments [17], but also confirms the good stability of gMC10 (Fig. S6).

The photocatalytic activities of bulk g-C_3N_4 and gMC10 were also evaluated according to the amount of H_2 generated from water splitting (Fig. 3c). The results show a large difference between the samples with and without the hole sacrifice agent triethanolamine (TEOA). Without TEOA, gMC10 generated 344.7 nmol H_2 after 24 h of irradiation, which indicates a 11.5 times higher photocatalytic activity than bulk g-C_3N_4 (29.8 nmol). In contrast, with TEOA, gMC10 generated only 99 nmol H_2 after 6 h of irradiation, while bulk g-C_3N_4 generated 1.61 μmol (16 times higher than the amount generated by gMC10). This phenomenon can be explained as follows: due to the addition of TEOA to the water-splitting system, the OH bond in TEOA also hydrogen bonded with the C═O moiety in gMC, which lead to electron transfer to TEOA instead of water. Therefore, gMC10 showed improved efficiency towards hydrogen production without TEOA but decreased efficiency compared with bulk g-C_3N_4 with TEOA. This adds further evidence for the existence of hydrogen bonding in the gMC samples.

Fig. 3d shows the linear sweep voltammetry (LSV) of g-C_3N_4 and gMC10 photocathodes in 0.5 M Na_2SO_4 solution. According to the photoelectrochemical measurements, the photocurrent of the gMC10 sample (3.63 μA cm^{-2}) was 3.5 times higher than that of g-C_3N_4 sample (1.07 μA cm^{-2}) at a potential of −0.02 V. Moreover, the onset potential for bulk g-C_3N_4 and gMC10 were 0.06 and 0.33 V vs Ag/AgCl, respectively. This clearly indicates that charge-carrier recombination is effectively decreased in gMC10 [18].

Typically, photoluminescence (PL) analysis is employed to investigate the migration, transfer and separation efficiency of photogenerated electrons and holes in a semiconductor, as the PL emission of a semiconductor mainly arises from charge-carrier recombination. Fig. 4a displays the PL spectra of the samples. The normalized PL spectra were acquired from the gMC powders using an excitation wavelength of 365 nm at room temperature. The main peak appearing at 466 nm in the spectrum of g-C_3N_4 blueshifted to 460.5, 460 and 458 nm with increasing concentration of the ammonia solution. On the other hand, a new peak appeared ca. 441 nm in the spectra of the gMC samples; moreover, the new peak in the gMC10 spectrum had a similar intensity to that of the main peak. This suggests that two band gaps exist in gMC10: one at 2.81 eV, and another at 2.70 eV. The conduction band of bulk g-C_3N_4 and gMC can be examined in detail in the Mott-Schottky plot. The positive slope of the Mott-Schottky plot reveals the n-type semiconductor characteristics of all obtained samples. The conduction band potentials of the samples were calculated to be −1.32 V vs. Ag/AgCl at pH 6.7, and this value did not change even with gMC10 (Fig. 4b). Therefore, gMC10 shows +1.49 V and +1.38 V valence bands, indicating a deeper valence band formed upon O 2p orbital hybridization in MC (Fig. S7) [19]. The conduction band of MC was located at +1.48 V vs. Ag/AgCl at pH 6.7 in the UPS analysis (Fig. S8), which is similar to the result calculated from the Mott-Schottky plot. Therefore, two mechanisms can possibly proceed in gMC: O doping in gMC and photoexcited hole transfer from the valence band to the deeper valence band. To confirm the mechanism, MC and g-C_3N_4 were finely ground by a mortar in a 1:1 wt percentage. Interestingly, CO_2 generation from the 1:1 sample reached 215 ppm after 24 h, which is almost 2.6 times higher than that from bulk g-C_3N_4 (Fig. S9). Since MC cannot absorb light (300–800 nm, Fig. 1d), only the g-C_3N_4 moiety in the composite can photoexcite hole-electron pairs. The enhancement in the photocatalytic activity the manually ground sample suggests that gMC allow a second mechanism in which photoexcited holes transfer from the valence band to the deeper valence band. However, theoretically, holes cannot be transferred from low to high valence bands

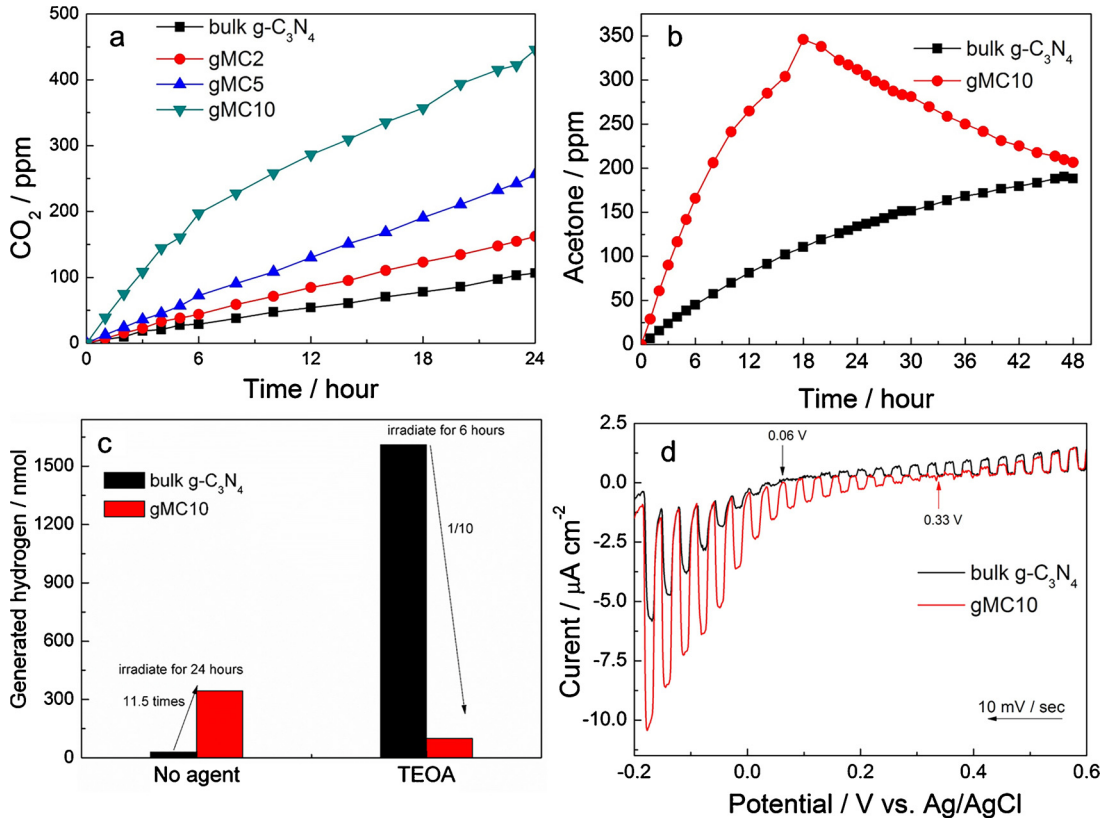

Fig. 3. Time evolution of (a) CO_2 generation from acetaldehyde decomposition and (b) acetone generation from 2-propanol decomposition under LED435 (3 mW/cm^{-2}) irradiation. (c) The amount of hydrogen generated under λ ≥ 420 nm (100 mW/cm^{-2}) irradiation without TEOA (24 h) and with TEOA (6 h). (d) Linear sweep voltammetry of bulk g-C_3N_4 and gMC10 electrodes under simulated solar (100 mW/cm^{-2}) irradiation.

unless there is sufficient driving energy.

From the FTIR results (Fig. 1b), both MC and gMC show broad peaks between 2625–2930 cm^{-1}, attributed to C═OH—N hydrogen bonds [20]. The hydrogen-bond peaks of MC are located at approximately 2697 and 2825 cm^{-1}, while those of gMC are located at approximately 2752 and 2853 cm^{-1}. These differences suggest that a large part of the C═OH—N hydrogen bond in gMC probably originated between g-C_3N_4 and MC. It is easier to form a hydrogen bond between C═O and H—N than C—N and H—N [8,9]; thus, during hydrothermal treatment (as well as during manual grinding), a C═OH—N hydrogen bond formed between g-C_3N_4 and MC. These results suggest that the driving energy may originate from the C═OH—N hydrogen bond.

In order to determine the charge transfer on the hydrogen bond, ^1H solid state NMR and in-situ FTIR analysis were employed. Fig. 5a presents the ^1H NMR spectra of g-C_3N_4 and gMC10. Two resolved peaks are visible for g-C_3N_4, which are located at 3.8 ppm (residual water) and 8.8 ppm (amino group) [21,22]. For gMC10, three peaks at 4.8 ppm (residual water), 9.6 ppm (amino group) and 14.8 ppm ($(C)_2NH$ from melamine cyanurate) are clearly resolved [23]. The amino group peak shows a low-field shift compared to g-C_3N_4, which can be attributed to the formation of hydrogen bond. Meanwhile, the intensity of amino group peak shows a gradual decrease because of the enhanced proton exchange process in NHO═C [24]. On the other hand, for in-situ FTIR analysis, as shown in Fig. 5b, the peaks originating from NHO═C hydrogen bond at 2752 and 2853 cm^{-1} become broader as from 200 °C in the warm-up process, which indicates that the thermal energy breaks the hydrogen bond. In the cool-down process, the hydrogen bond recovers when the temperature is lower than 200 °C (Fig. 5c), and the

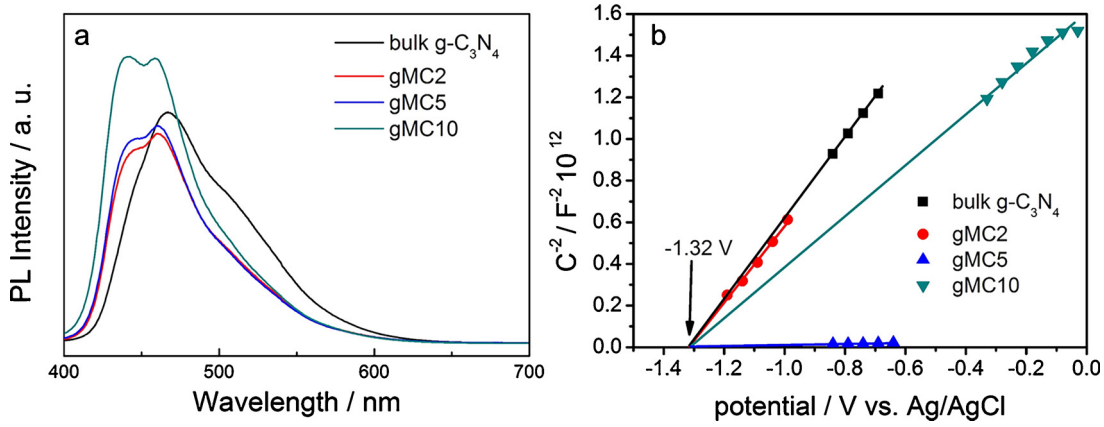

Fig. 4. (a) Photoluminescence spectra and (b) Mott-Schottky plots of the obtained samples.

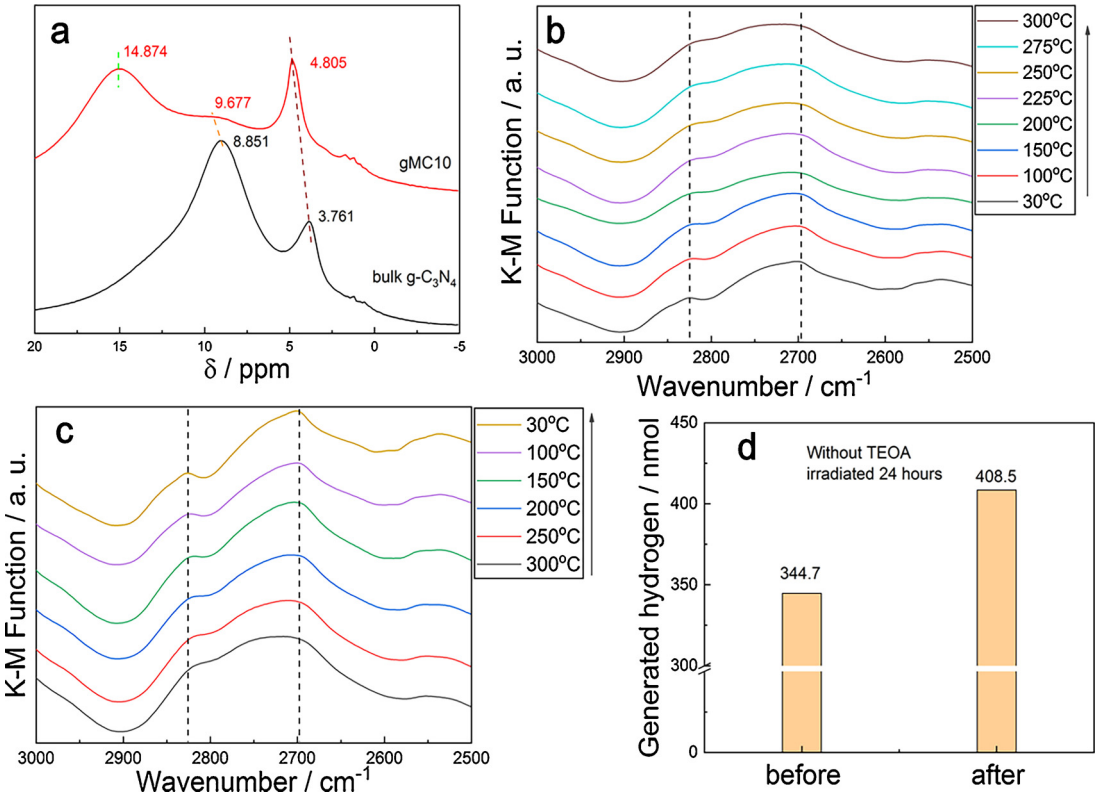

Fig. 5. (a) ^{1}H MAS solid-state NMR spectra for g-C_3N_4 and gMC10. In-situ FTIR spectra (b) warm-up process and (c) cool-down process for gMC10. (d) The amount of hydrogen generated under λ ≥ 420 nm (100 mW/cm^{-2}) irradiation without TEOA for gMC10 sample before and after calcination (3 h under 200 °C).

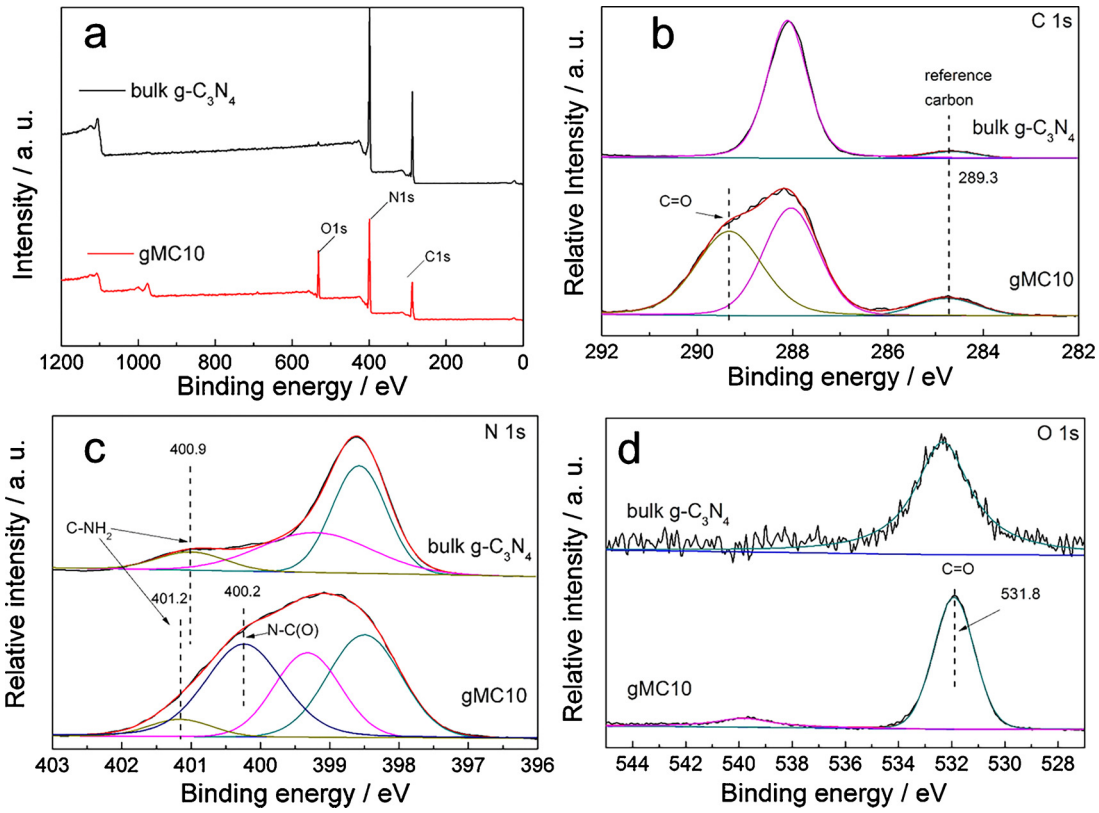

Fig. 6. (a) Survey spectra, (b) C 1s, (c) O 1s and (d) N 1s XPS spectra of bulk g-C_3N_4 and gMC10.

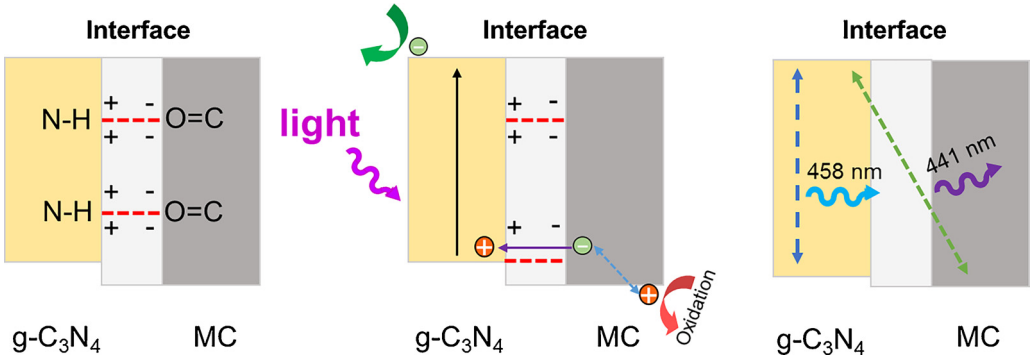

Fig. 7. Proposed mechanism of electron transfer via the hydrogen bonding and PL quenching process of the gMC nanocomposite.

peaks at 2752 and 2853 cm^{-1} become more significant than the original state. According to the results of in-situ FTIR analysis, as shown in Fig. 5d, gMC10 calcined for 3 h at 200 °C presents higher photocatalytic activity (408.5 nmol) than the gMC10 without calcined (344.7 nmol). The result suggests that the hydrogen bond plays a key role in the gMC and ordered hydrogen bond is beneficial to improve the photocatalytic activity. The results of ^{1}H solid state NMR and in-situ FTIR analysis provide the circumstantial evidences for charge transfer that can be assisted by the hydrogen bond.

To determine the behavior of the C═OH—N hydrogen bonds in gMC, XPS analysis was performed. The XPS survey spectra of the samples show the presence of C 1s, N 1s, and O 1s peaks. A strong oxygen peak is detected in gMC10, indicating that gMC10 had a higher oxygen content (Fig. 6a), which corresponds with the element analysis (Table 1). A new peak appeared in the high-resolution C 1s core-level spectrum of gMC10 (Fig. 6b), compared with that of bulk g-C_3N_4, which is assigned to carbonyl carbons (BE = 289.3 eV). The C═O peak can also be seen in the high-resolution O 1s core-level spectrum (Fig. 6d) at 531.8 eV, with a 0.3 eV shift to a lower binding energy than that of the carbonyl oxygens (BE = 532.1) [25]. The high-resolution N 1s core-level spectra (Fig. 6c) of bulk g-C_3N_4 and gMC10 are composed of three and four features, respectively. The peaks at 398.5, 399.2 and 400.9 eV in the spectrum of bulk g-C_3N_4 are derived from the C—N═C, N—$(C)_3$ and amino groups [26]. Compared with bulk g-C_3N_4, the peaks in the gMC10 spectrum showed a slight shift to 398.4, 399.3 and 401.2 eV, respectively. (The new peak in the gMC10 spectrum at 400.2 eV can be ascribed to C═O.) The peak derived from the amino group N shifted by 0.3 eV to higher binding energy, and the carbonyl oxygen O peak shifted by 0.3 eV to lower binding energy. These results suggest the existence of N—HO═C hydrogen bonds in the gMC10 sample as well as electron accumulation at the O side and hole accumulation at the N side after formation of the N—HO═C bonds. Therefore, before light irradiation, electron-hole diffusion will form a so-called inner electric field between the two ends (g-C_3N_4 and MC) of the hydrogen bond. When gMC is irradiated by incident light, the g-C_3N_4 moiety can be excited, generating electron-hole pairs. The photogenerated holes will recombine with the electrons from the MC moiety due to the inner electric field [27], leaving electrons in the CB of g-C_3N_4 moiety and holes in the MC moiety, which results in separation of the electron-hole pairs (Fig. 7). From the XPS results, it can be confirmed that hydrogen bonds provide an ultrafast pathway not only because hydrogen bonds are shorter than van der Waals junctions but also because of the inner electric field formed between the two ends of the hydrogen bond.

The time-resolved fluorescence decay spectra based on Fig. 4b was used to investigate the behavior of photoexcited charge carriers. As shown in Fig. S10, $\tau 1$ of g-C_3N_4 increases from 1.50 ns (65.2%) to 1.73 ns (42.61%), simultaneously $\tau 2$ decreases from 9.91 ns (34.8%) to 9.37 ns (57.39%) compared to that of gMC10. Considering the PL results, a possible mechanism is shown in Fig. 7. The pathway for excited charges that the hydrogen bonds provide is directional; therefore, the interfacial barrier between g-C_3N_4 and MC influences the lifetime. This mechanism requires the existence of holes in the deeper valance band, which are provided by the O 2p orbital.

4. Conclusion

In this article, hydrogen bond-based composite gMC samples were fabricated by the hydrothermal treatment of g-C_3N_4 in ammonia solution. The gMC samples show improved photocatalytic activity towards the decomposition of acetaldehyde and 2-propanol as well as photocatalytic water splitting. It is demonstrated that hydrogen bonds are formed between g-C_3N_4 and MC, which provide an electronic field for electrons transfer from MC to g-C_3N_4. Therefore, MC becomes the oxidation site, and g-C_3N_4 becomes the reduction site, which allows the efficient separation of hole-electron pairs. Recently, MC has been used to improve the stability of unstable 2D materials, which is probably due to the behavior of the hydrogen bonds [28]. Hydrogen bonding offers a new route to lower the interfacial barrier at the heterojunction; moreover, the directionality of the hydrogen bond offers the possibility to design heterojunction photocatalysts that function through the expected mechanism.

Acknowledgements

This work was supported by the National Natural Science Foundation of China under Grant Nos. 51502178, the Shenzhen Science and Technology Project under Grant Nos. JCYJ20170412105400428, KQJSCX20170727101208249 and JCYJ20160520174909208 and the Natural Science Foundation of SZU.

Appendix A. Supplementary data

Supplementary material related to this article can be found, in the online version, at doi: https://doi.org/10.1016/j.apcatb.2018.04.057.

References

[1] Q. Wang, T. Hisatomi, Y. Suzuki, Z. Pan, J. Seo, M. Katayama, T. Minegishi, H. Nishiyama, T. Takata, K. Seki, A. Kudo, T. Yamada, K. Domen, J. Am. Chem. Soc. 139 (2017) 1675–1683.
[2] K. Tsuji, O. Tomita, M. Higashi, R. Abe, ChemSusChem 9 (2016) 2201–2208.
[3] Z. Jin, N. Murakami, T. Tsubota, T. Ohno, Appl. Catal. B-Environ. 150–151 (2014) 479–485.
[4] Q. Wang, T. Hisatomi, Q. Jia, H. Tokudome, M. Zhong, C. Wang, Z. Pan, T. Takata, M. Nakabayashi, N. Shibata, Y. Li, I.D. Sharp, A. Kudo, T. Yamada, K. Domen, Nat. Mater. 15 (2016) 611–615.
[5] Q. Xiang, J. Yu, M. Jaroniec, J. Phys. Chem. C 115 (2011) 7355–7363.
[6] J. Low, J. Yu, M. Jaroniec, S. Wageh, A.A. Al-Ghamdi, Adv. Mater. 29 (2017) 1601694–1601713.
[7] T. Hisatomi, J. Kubota, K. Domen, Chem. Soc. Rev. 43 (2014) 7520–7535.
[8] G.R. Desiraju, Acc. Chem. Res. 35 (2002) 565–573.
[9] G.-J. Zhao, K.-L. Han, Acc. Chem. Res. 45 (2012) 404–413.
[10] C.F. Guerra, F.M. Bickelhaupt, J.G. Snijders, E.J. Baerends, Chem.–Eur. J. 5 (1999) 3581–3594.

[11] T. Nishino, N. Hayashi, P.T. Bui, J. Am. Chem. Soc. 135 (2013) 4592–4595.
[12] V. Quaranta, M. Hellström, J. Behler, J. Phys. Chem. Lett. 8 (2017) 1476–1483.
[13] Y. Su, Z. Han, L. Zhang, W. Wang, M. Duan, X. Li, Y. Zheng, Y. Wang, X. Lei, Appl. Catal. B-Environ. 217 (2017) 108–114.
[14] C. Wang, Y. Fu, L. Zhang, D. Danovich, S. Shaik, Y. Mo, J. Comput. Chem. 39 (2018) 481–487.
[15] Y.-S. Jun, E.Z. Lee, X. Wang, W.H. Hong, G.D. Stucky, A. Thomas, Adv. Funct. Mater. 23 (2013) 3661–3667.
[16] M. Shalom, S. Inal, C. Fettkenhauer, D. Neher, M. Antonietti, J. Am. Chem. Soc. 135 (2013) 7118–7121.
[17] Q. Zhang, B. Xu, S. Yuan, M. Zhang, T. Ohno, Catal. Today 284 (2017) 27–36.
[18] J.A. Seabold, K.-S. Choi, Chem. Mater. 23 (2011) 1105–1112.
[19] D.E. Scaife, Sol. Energy 25 (1980) 41–54.
[20] A. Ranganathan, V.R. Pedireddi, C.N.R. Rao, J. Am. Chem. Soc. 121 (1999) 1752–1753.
[21] B. Gr¨unberg, T. Emmler, E. Gedat, I. Shenderovich, G.H. Findenegg, H. Limbach, G. Buntkowsky, Chem.–Eur. J. 10 (2004) 5689–5696.
[22] A. Sattler, S. Pagano, M. Zeuner, A. Zurawski, D. Gunzelmann, J. Senker, K. M¨uller-Buschbaum, W. Schnick, Chem.–Eur. J. 15 (2009) 13161–13170.
[23] K. Damodaran, G.J. Sanjayan, P.R. Rajamohanan, S. Ganapathy, K.N. Ganesh, Org. Lett. 3 (2001) 1921–1924.
[24] X.L. Wang, W.Q. Fang, H.F. Wang, H. Zhang, H. Zhao, Y. Yao, H.G. Yang, J. Mater. Chem. A 1 (2013) 14089–14096.
[25] Y. Tooru, Y. Kiyoshi, S. Shigemasa, Bull. Chem. Soc. Jpn. 51 (1978) 1561–1562.
[26] R.C. Dante, F.M. Sánchez-Arévalo, P. Chamorro-Posada, J. Vázquez-Cabo, L. Huerta, L. Lartundo-Rojas, J. Santoyo-Salazar, O. Solorza-Feria, J. Solid State Chem. 226 (2015) 170–178.
[27] Z. Jin, Q. Zhang, L. Hu, J. Chen, X. Cheng, Y.-J. Zeng, S. Ruan, T. Ohno, Appl. Catal. B-Environ. 205 (2017) 569–575.
[28] V.V. Korolkov, I.G. Timokhin, R. Haubrichs, E.F. Smith, L. Yang, S. Yang, N.R. Champness, M. Schröder, P.H. Beton, Nat. Commun. 8 (2017) 1385–1392.